Interpretation of Geomaterial Behavior during Shearing Aided by PIV Technology

Interpretation of Geo-material Behavior during Shearing aided by PIV Technology

Peerun, M.I.[1], Ong, D.E.L.[2*], Choo, C.S.[3]

[1]PhD Scholar, Griffith University, School of Engineering and Built Environment, 170 Kessels Road, Nathan, Queensland 4111, Australia. Email: irfaan.peerun@griffithuni.edu.au

[2]Senior Lecturer, Griffith University, School of Engineering and Built Environment, 170 Kessels Road, Nathan, Queensland 4111, Australia and Adjunct Associate Professor, Swinburne University of Technology Sarawak Campus, 93350 Kuching, Sarawak, Malaysia. Email: d.ong@griffith.edu.au

[3]Senior Lecturer, Centre for Sustainable Technologies, Faculty of Engineering, Science & Computing, Swinburne University of Technology Sarawak Campus, 93350 Kuching, Sarawak, Malaysia. Email: cschoo@swinburne.edu.my

*Corresponding author:
Name: D. E. L. Ong
Address: Senior Lecturer, Griffith University, School of Engineering and Built Environment, 170 Kessels Road, Nathan, Queensland 4111, Australia
E-mail: d.ong@griffith.edu.au

Abstract

Several researchers have studied the behavior of particles during shearing to have better insight on the Mohr-Coulomb (MC) strength parameters. In most cases, the movements of particles along the shear band were studied by means of numerical modeling to obtain the velocities and directions of the soil particles. The use of a transparent shear box highlights the original enhancement and contribution in this paper to study the mechanical behavior of particles using particle image velocimetry (PIV) along the shear zone. Earlier literature on research utilizing "transparent shear box" consisted of several limitations such as obstructed view of the shear zone or using numerical simulation. The tested specimens consisted of sand and reconstituted rock spoils of metagreywacke and shale origins, which were classified according to their shapes and mineralogy contents. Particle shearing behavior were analyzed in detail at various stages throughout the direct shear tests with results complementing the PIV assessments. This novel interpretation technique has successfully demonstrated how particle shapes and angularity, mineralogy as well as effects of particle dilation and compression under shear, can influence the strength parameters.

Keywords: Apparent cohesion, Direct shear, GeoPIV, Dilation, Compression,

Introduction

Particle behavior along shear bands has been studied by many researchers. In order to obtain better insights into particle behavior during shearing, laboratory tests and numerical modeling are usually performed. However, in the course of such studies, many limitations were identified. These limitations include (i) non-uniformities of stress produced during direct shear testing being apparent only through numerical simulations (Potts et al. 1987, Indraratna et al. 2014); (ii) views of shear zones being obstructed due to equipment fittings (Fukuoka et al. 2006); (iii) isolated discontinuous observations of shear band development and particulate activities (Wang and Sassa 2002, Wafiq et. Al 2004); and (iv) studies being limited to plane-strain assumptions of granular specimens (Yuan et. al 2017).

The limitations showed that there is a need for physical tests to act as crucial experimental validation of simulated particle behaviors, and to provide continuous and unobstructed views of granular materials when subjected to shearing. Therefore, in order to address the shortcomings highlighted earlier, it is crucial to acquire clear evidence of the test specimens during shearing for the analysis of particle movements along the shear zone. In the current study, this was achieved through the acquisition of continuous sequential high-resolution images from direct shear tests performed on actual granular materials by using a fully transparent shear box. The authors agree that PIV is not a new technique, but the supplementary use of PIV in validating a usual shear box test and subsequently with interpreted parameters and techniques developed for the accurate analyses of real-life pipe-jacking works (Choo and Ong 2015, 2017; Ong and Choo 2016, 2018), is indeed original and important in advancing fundamental understanding in this research area. Usually the shear box is considered as a ‘black box’ due to the unknown particle interaction and only the results can be relied on. Previous studies conducted partial analysis or numerical simulation while this study is unique where for

63 the first time, the best judgement can be made about particles behavior along the shear zone
64 unobstructed, using the transparent shear box.

65 This paper discusses the contributions of particle image velocimetry (PIV) technology in
66 providing better insights to particle behavior during shear and how this phenomenon affects
67 the Mohr-Coulomb strength parameters. This was achieved by studying the mechanical
68 behavior of granular soils during different shearing stages using a purpose-built, transparent
69 shear box and with the aid of PIV technique to analyze particle movements in the shear box.
70 The transparent shear box gives a technical enhancement to this study, where all activities along
71 the shear band can be captured via continuous sequential images throughout the tests. The well-
72 calibrated PIV method is then used to analyze the images acquired during the shearing process
73 of the specimens at various well-defined stages, namely (i) end zone deformation, (ii) particle
74 interlocking, (iii) shear zone formation and (iv) steady shear (Li and Aydin 2010). The PIV
75 analyses and outcomes were then used to interpret the direct shear test results in order to
76 develop detailed understanding of how the Mohr-Coulomb parameters could be influenced by
77 a typical geology, mineralogical content, particle shape and angularity as well as effects of
78 particle dilation and compression during shear under various normal stresses.

79 ***Tested Materials***

80 Three types of granular materials were chosen as testing specimens, namely sand,
81 metagreywacke spoils and shale spoils. Well-graded sand was used while spoils of
82 metagreywacke and shale origins were obtained from various sites in Kuching city, on the
83 island of Borneo. The sand was classified as rounded and sub-angular smooth particles with
84 main constituent of quartz, whereas metagreywacke and shale particles were more angular and
85 had rougher surfaces.

Petrographic analyses carried out on sand showed that sand can be considered as orthoquartzite, where the high content of pure quartz cemented by silica produces extremely strong particles (Pfeffer 2014). Petrographic analyses also showed that metagreywacke sample comprised of poorly sorted angular to subangular quartz grains, feldspar grains and rock fragments in a matrix of fine-grained quartz, sericite, chlorite and clay minerals. Shale being more fissile (can be easily split apart), is more prone to weathering effects that makes it relatively weaker (Pfeffer 2014). Shale spoils comprised mainly of clay minerals, silt-sized quartz grains, tiny flakes of mica and carbonaceous materials.

The test specimens were oven-dried and scalped with a distribution of particle sizes passing 2.36 mm sieve and retained by 75 μm sieve according to Section 6.2.1 – 6.2.3 of ASTM D 3080 / D3080M-11(2011) Standard Test Method for Direct Shear Test of Soils Under Consolidated Drained Conditions (ASTM 2011a). The scalping method consists of removing particle sizes beyond the allowable particle size range for the test specimen. The scalping method was previously adopted by Choo and Ong (2015) during direct shear testing of reconstituted rock spoils. Fig. 1 shows the particle size distribution curves for the tested specimens.

The specimens consisted of sand-sized grains and can thus be classified as well-graded sand and poorly graded rock spoils (metagreywacke and shale) according to ASTM D2487-11 Standard Practice for Classification of Soils for Engineering Purposes (Unified Soil Classification System) (ASTM 2011). Dry density was obtained by computing the specimen dry mass and the initial specimen volume. Table 1 shows the physical properties of the test specimens.

Direct Shear Testing

Direct shear tests were conducted on each specimen according to ASTM D3080 / 3080M-11(2011) Standard Test Method for Direct Shear Test of Soils Under Consolidated Drained Conditions (ASTM 2011a) in order to obtain their strength characteristics. A series of direct shear test was conducted for each specimen with sample size of 63.3 mm diameter and 27 mm height at normal stresses of 100 kPa, 200 kPa, 300 kPa, 400 kPa and 500 kPa. Using a fully-automated direct shear equipment, each specimen was sheared at constant rate of 0.0017 mm/s for a horizontal displacement of 15 mm.

To understand the particle behavior during shearing, the four-stage shearing model developed by Li and Aydin (2010) was used as a guideline to interpret the direct shear test results. It is hoped that better insights could be made to understand the apparent cohesion and frictional angle values of different sets of geology based on their respective particle shapes and mineralogy contents.

Understanding the Shearing Stages

Theoretically, at the start of the shearing phase, the sample is in a contraction phase. The particles, especially those along the shear band, rearrange themselves into the existing voids, resulting in contraction. This first stage during shearing is called “end zone deformation”, which will end at the lowest point in volumetric strain, where particles are thought to be interlocking one another to stop further contraction (Shimizu 1997). During the second stage of shearing known as “particle interlocking” stage, the particles along the shear band have to surpass interlocking by rolling on the surrounding particles. This will result in localized dilation and hence volumetric strain will increase. Peak stress is achieved when particle movements are fully mobilized at the maximum interlocking phase within the shear band. “Shear zone formation” is the third stage during the shearing process, which starts from the peak stress until a constant stress level is achieved. The shear band develops more actively due to particle

movements and this results in a looser layer (Oda and Kunishi 1974; Fukuoka et al. 2006). Along the shear band, the smaller particles tend to rearrange themselves by filling the voids and larger particles will roll or rotate. This will allow the shear zone to readjust its structure and cause reduction in the shear resistance. The last stage of shearing is when "steady shear" occurs, where regular but uneven layers of particles are locked into the structure of the layer. The structure at the upper half of the shear box remains steady while the lower half moves forward at constant amplitude with negligible vertical displacement. At this point, the particles would tend to slide along the upper and lower block interfaces with an effective balance of dilation and contraction. Hence, no significant dilation occurs at this stage and hereafter, the test specimen moves with minimal vertical deformation to reach a residual state (Li and Aydin 2010).

Experimental Setup

In order to study particle behavior during shearing, a purpose-built shear box was fabricated using Perspex, a transparent material that allows clear visibility of the particles. The shape and dimensions of the Perspex shear box are identical as compared to a conventional shear box with accordance with ASTM D3080 / D3080M-11(2011) Standard Test Method for Direct Shear Test of Soils Under Consolidated Drained Conditions (ASTM 2011a). Fig. 2 shows the drawing specifications for the (a) top half and (b) bottom half of the Perspex shear box. Although having relatively lower rigidity, acrylic has been successfully used in previous research works consisting of shearing. Fukuoka et al (2006) used acrylic to fabricate a transparent ring shear box to study shear zone formation for granular materials. However, due to the equipment constraint, part of the shear zone was obstructed by a steel plate. Sharma et al (2007) conducted interface shearing between silty sand and geomembrane. The interface material was achieved by using an acrylic block of 100 mm x 100 mm x 38 mm and the geomembrane was glued onto it. In this study, constant normal stress was achieved during

158 shearing which demonstrate that the acrylic shear box is strong and stable throughout the test.
159 Any deformation would result into cracks within the shear box, which was not noticeable after
160 conducting tests at maximum load of 500 kPa. The shear stress obtained is purely from the test
161 specimen and not in contact with the shear box which is ensured by the allocated shear gap of
162 0.63 mm.

163 ***Particle Image Velocimetry (PIV)***

164 Particle image velocimetry is a technique developed to measure velocity by using double-flash
165 photography (Adrian 1991). The method consists of analyzing a series of sequential images
166 during a seeded flow using an autocorrelation function to produce displacement vectors.
167 GeoPIV is a MATLAB module, which executes PIV in geotechnical testing applications. It
168 uses the principles of PIV to capture vector displacement during geotechnical testing. The
169 texture of the tested soil specimen can be tracked through a batch of images to produce a
170 complete vector trajectories plot of the test specimen (White and Take 2002, White et al 2003).
171 GeoPIV can be used to help develop understanding on the dynamics of particles in the shear
172 box. Localized activities such as dilation and compression, which are due to particle behavior
173 during shear can be observed. Although the software cannot quantify such localized activities,
174 it provides a good representation of the particle movements for better visualization when
175 evaluating particle behavior in conjunction with the shearing test results. Therefore, better
176 understanding and judgement on particle behavior and strength development can be developed.
177 GeoPIV uses the first image as the reference point and compares the subsequent images with
178 the first reference image to produce relative displacement between the images. Hence, as stated
179 by Mehdizadeth et al (2015), any possible distortion due to curvature, camera lens and light
180 refraction are eliminated.

181 ***Testing Procedure***

182 *Sample Preparation*

183 The specimens were poured into the shear box by means of dry pluviation method, using a
184 funnel of 0.35 mm opening diameter and a fall height of 100 mm, to achieve a dense sample
185 (DeGregorio 1990). Dry pluviation method was adopted to ensure consistency within the test
186 samples where constant weight and void ratio was achieved for each specimen. From Table 1,
187 sand produced the highest dry density, followed by metagreywacke and shale being the least
188 dense specimen. Each material was reconstituted and sheared at 100 kPa, 200 kPa, 300 kPa,
189 400 kPa, and 500 kPa normal stresses. The range of normal stresses was adopted to demonstrate
190 the changes in particles behavior at varying normal stresses from relatively low to high stresses
191 and to also represent the depth of the jacking process performed in the field.

192 *Image Acquisition*

193 Sequential images were captured at an interval of 150 s while the specimen was subjected to
194 shear for a maximum displacement of 15 mm. The images were remotely taken using a Canon
195 EOS 450D camera with linear kit lens. Fig. 3 shows the image acquisition with the highlighted
196 region of interest (ROI). A larger image resolution will produce greater number of patches and
197 hence more information can be obtained (Grognet 2011). The images obtained from the camera
198 were of 72 dpi resolution, with dimensions of 4272 × 2848 pixels and a region of interest as
199 shown in Fig. 3.

200 Naturally textured soils like sand which consist of various grain colors, does not require
201 addition modification to produce pseudotexture as opposed to clayey soils (Mirzababaei et al
202 2017). Hence, no markers or dyed particles were added to the tested specimens. To avoid any
203 possible light reflection or shaded area on the transparent shear box, light shades were placed
204 near the shear box. The dim lighting condition was maintained constant throughout the tests
205 while other sources of lights were restricted. This was to ensure suitable images with consistent
206 light density were obtained for GeoPIV analyses.

The Region of Interest (ROI) was set between the upper half and lower half of the shear box since particle activities such as interlocking and rolling occur along the shear zone. Such activities are used to justify the specimen's apparent cohesion and friction angle. Similar approach was made by Fukuoka et al (2006) where image processing was used to measure velocity distribution within shear zone during ring shear tests. A predetermined shear plane of 4.0 cm thickness was studied for a sample height of 11 cm. Obtaining a 2D section view representation of the particle mechanism during shearing is the most realistic approach while a 3D view of the particles can only be achieved through numerical simulation and not an actual physical test. DeJong and Westgate (2009) have previously used a section view of the shear box to describe localized soil-structure interaction during a batch of interface shear tests. Vangla and Gali (2015) adopted similar side view of the shear box to demonstrate shear band formation during interface shearing tests. Fukuoka et al (2006) used video image analysis to study the shear-zone formation of granular materials during a series of ring shear test using a transparent shear box. Hence, the 2D section-view was analyzed and thus can confidently represent particle activities within the whole specimen.

The size and position of the ROI were maintained for all the tests. To convert the image-space coordinates into object-space coordinates during PIV analysis, a set of reference targets with its known object-space coordinates is required (White et al 2003). As seen in Fig. 3, the grids above and below the Region of interest (ROI) were purposely placed and with known dimension of 5 mm by 5 mm to facilitate the conversion from pixel to mm. The measurement precision error, ρ obtained was 0.038 with 47526 measurement points, n which is acceptable due to its low precision error and yet larger number of measurement points (Peerun et al 2016, Peerun, M. I. 2016).

Results

Direct shear test results

Figs. 4 (a), (b) and (c) show the shear stress and volumetric plots for well-graded sand, metagreywacke and shale, respectively. Well-graded sand showed distinct peak shear stress and produced a constant residual shear stress state. Almost no compression was found at the initial shearing stage, followed by dilation at Stage 2 and compression to almost zero vertical displacement at the end stage of shearing. Metagreywacke and shale spoils exhibited similar trends at different normal stresses but with less distinct peak stresses compared to results from tests on sand. The samples were compressed to a maximum vertical displacement of 0.45 mm. With increasing normal stress, dilation was reduced significantly.

Metagreywacke and shale produced higher residual shear stresses (for metagreywacke, $\tau_{residual}$ = 355.3 kPa; for shale, $\tau_{residual}$ = 359.5 kPa) as opposed to sand ($\tau_{residual}$ = 292.1 kPa), which was expected as metagreywacke and shale consisted of angular particles with higher surface roughness. As mentioned by Djipov (2012), angular particles when subjected to compression were prone to breakages. Therefore, it is consistent to note that at the highest normal stress, spoils of metagreywacke and shale achieved a maximum vertical compression of 0.46 mm and 0.53 mm, respectively, whereas sand compressed vertically by only 0.06 mm. This could mean that poorly sorted angular shale particles were more prone to breakages during the shearing process. Dilatancy angle, ψ was computed from Eq. (1), as defined by Bolton (1986).

$$\tan\psi = -\frac{\mathrm{d}\,\varepsilon_y}{d\gamma_{yz}} \tag{1}$$

where ε_y is the vertical strain and γ_{yz} is the shear strain. Both parameters were measured at the occurrence of peak shear stresses during the tests. A positive value of ψ would indicate dilating behavior while a negative value would show contracting behavior of the specimen. Table 2 shows that sand produced greater dilatancy angle, while metagreywacke and shale produced relatively lower dilatancy angles and exhibited compression at higher normal stresses. A

255 reduction in dilatancy angle was observed with increasing normal stress. Similar observations
256 could be made from Fig. 4, where sand specimens demonstrated dilation while metagreywacke
257 and shale specimen were compressed. At higher normal stresses, the specimens produced
258 greater compression, which was also demonstrated by a reduction in dilatancy angle, as
259 reported in Table 2.

260 *Void Ratio*

261 Void ratio was used to quantify which specimen dilated or compressed more during the direct
262 shear test. The void ratio was calculated before and after the test. Due to the sample preparation
263 method, the initial weights were constant. The initial void ratio was obtained from Eq. (2) (Das
264 2008), where G_s is the specific gravity, γ_w is the unit weight of water and γ_d is the dry unit
265 weight of the specimen.

266 $$Initial\ void\ ratio = \frac{G_s \times \gamma_w}{\gamma_d} - 1 \quad (2)$$

267 The void ratio after the direct shear test was computed based on the change in specimen height
268 due to dilation or compression. Hence, producing a change in specimen volume. Table 3 shows
269 the void ratio before and after direct shear test for the tested specimens.

270 Figs. 5 (a), (b) and (c) show the strength envelopes for sand, metagreywacke and shale,
271 respectively. Choo and Ong (2015) found that by using the best-fit MC strength criterion, over-
272 estimation of shear strength may occur at lower and higher normal stresses, while under-
273 estimation occurs at intermediate stresses for materials with non-linear strength development.
274 Therefore, to avoid these potential inaccuracies, a power law function was used for
275 characterizing non-linear shear strength behavior of tested samples (De Mello, 1977). The
276 simplified power-type function is defined as

277 $$\tau = A \,.\, (\sigma')^B \quad (3)$$

where A is a dimensionless constant that governs the magnitude of the power function and B is a dimensionless constant that governs the curvature of the power function (Choo and Ong 2017). Since the MC strength parameters are usually required, a generalized tangential technique proposed by Yang and Yin (2004) was used to define the internal frictional angle and cohesion of the tested specimens. This technique requires a tangent to the power law strength envelope to be drawn at the desired in-situ pressure to obtain the corresponding MC parameters. The power law function was applied to sand and metagreywacke as the strength envelopes showed non-linearity. Tangents were drawn at 100 kPa, 300 kPa and 500 kPa for peak and residual stresses, to demonstrate the difference in tangential MC parameters between low and high normal stresses. This technique has been successfully used by Choo and Ong (2015) as well as Ong and Choo (2016) to interpret the c' and ϕ' values of reconstituted rock spoils. For the shale specimens, additional tests were performed at low normal stresses (25 kPa, 50 kPa, 75 kPa and 100 kPa) in order to ascertain whether the tested shale demonstrated any possible nonlinearity in its stress-strain behavior. The eight tests on reconstituted shale specimens produced a linear behavior even when using the power law function. Hence, a MC plot was sufficient to obtain the friction angle and cohesion of shale. Similar linear behavior was observed for shale by Choo and Ong (2015). An apparent cohesion of $c' = 0$ suggested that particle breakage was significant, with little to no interlocking. This was due to the presence of angular flaky mica and sericite minerals, which are susceptible to particle breakage (Choo and Ong, 2015; Ong and Choo, 2018). This was corroborated by the minimal dilation demonstrated throughout the tests, culminating in overall volumetric compression by the end of each test on shale. By using MC, a constant value of internal friction angle is obtained as opposed to the tangential technique. The friction angle for shale remained unchanged when tested at varying normal stresses because of the absence of any significant apparent cohesion.

Table 2 presents the comparison results of the MC parameters at peak and residual state for sand, metagreywacke and shale.

It is apparent that an increase in normal stresses will produce higher apparent cohesion with a corresponding reduction in frictional angle. In this study, the cohesion *c'*, is described as an apparent cohesion instead of a true cohesion. Taylor (1948) defined apparent cohesion as a product of interlocking which is applicable to all types of soil such as clay and gravel. Lu et al (2009) recorded a small amount of apparent cohesion for dry sand based on the stress range. The test specimens were oven-dried and sheared in dry state. Using a linear representation to define the true soil strength behavior of a nonlinear material would be highly reliant on the applied normal stress (Choo 2015). Hence, using 'standard' Mohr-Coulomb failure criterion would unnaturally force the selection of zero cohesion and will lead to inaccurate prediction of jacking forces in a mass of bedrock in the field. Therefore, it is recommended that the tangential approach developed by Yang and Yin (2004) is to be adopted to obtain the apparent cohesion at specific normal stress. This methodology has been successfully used by Choo and Ong (2015, 2017), Ong and Choo (2016, 2018).

Sand exhibited relatively higher apparent cohesion as opposed to metagreywacke. This can be explained due to its coarser particles as opposed to metagreywacke and shale. The strong quartz consitituents of the sand sample produced greater interlocking and thus, higher apparent cohesion. On the other hand, the matrix of fine-grained quartz, sericite, chlorite and clay minerals from metagreywacke shows that the particles were much weaker and could possibly be prone to breakages. Shale consisted mainly of fine-grained clay minerals, silt-sized quartz grains, tiny flakes of mica and carbonaceous materials, which produced minimal cohesion as compared to the well-graded sand particles. At the highest applied normal stress, σ'_n of 500 kPa, shale spoils continued to demonstrate minimal apparent cohesion, suggesting that the

highly angular shale grains had minimal particulate strength. The observed peak apparent cohesion was zero, while a negative dilatancy angle was produced due to the vertical compression of the test specimen. These were further indications that spoils of shale were prone to particle breakage. For spoils of metagreywacke at a normal stress of 500 kPa, the peak apparent cohesion was 39.8 kPa before reducing to a residual apparent cohesion of 3.7 kPa. This suggests that particle breakage may have contributed to this reduction of residual apparent cohesion in the angular spoils of metagreywacke, resulting in an almost purely frictional material in the residual state. The negative dilatancy angle further supported the suggestion that metagreywacke spoils were susceptible to particle breakage.

These indications of particle breakage become apparent when the angular spoils of shale and metagreywacke were contrasted against sand. For sand at a normal stress of 500 kPa, the peak apparent cohesion was highest at c' = 57.5 kPa. There was a reduction in apparent cohesion towards the residual state, however, this residual apparent cohesion of 18.6 kPa was significantly higher than those interpreted from tests on angular spoils of metagreywacke and shale. The dilatancy angle at this normal stress was 4.1°. This suggests that the particle breakage was less significant in the orthoquartzite sand, owing to the extremely strong quartz particles (Pfeiffer 2014). With these indications of particulate mechanics and strength for the orthoquartzite sand and the highly angular spoils of metagreywacke and shale, it was therefore crucial to gain further insight from GeoPIV analysis on the performed direct shear tests.

Particle Behavior During Shearing

Particle breakage could have a significant influence on the structural behavior of crushable granular soil. Particle hardness, shape and size are some external factors affecting particle crushability. Particles of greater hardness will be less susceptible to breakage. Angular particles will be expected to have more breakages, as the stresses are concentrated at the edges of the

particles. On the other hand, a well-graded sample is not expected to develop such behavior since it has less voids. Hence, higher void ratio and presence of angular particles in a sample tend to experience more breakages, which could be possible for metagreywacke and shale spoils. Due to the relatively small volume of particle breakages that might have occurred, meaningful evaluation of particle size distribution tests to investigate particle breakages could not be successfully achieved. Therefore, GeoPIV technique was used to demonstrate localized movements of particles such as dilation and compression which could provide clues to possible particle breakage or interlocking occurring within the shear box during the shearing process. It is the Authors' plan to perform Discrete Element Modeling (DEM) in the future to better understand the particle breakage or interlocking phenomenon.

GeoPIV Results

The most suitable set of GeoPIV parameters was defined by means of a calibration exercise and the measurement precision error, ρ obtained was 0.038 with 47526 measurement points, n which is acceptable due to its low precision error and yet larger number of measurement points (Peerun et al 2016, Peerun, M. I. 2016). Sequential images were captured during the shearing of sand, metagreywacke and shale at normal stresses of 25 kPa, 50 kPa, 75 kPa, 100 kPa, 200 kPa, 300 kPa, and 500 kPa. The GeoPIV software was used to analyze the images. GeoPIV vector plots were produced at each of the four shearing stages as refences to demonstrate particle movements.

Fig. 6 shows a typical vector plot for sand at normal stress of 500 kPa, during shearing at Stage 3 (shear displacement: 4.983 mm - 7.620 mm). The magnitude of particle movements are represented by arrows, whose lengths are proportional to the magnitudes of each respective displacement. The upper and lower halves of the shear box can be easily distinguished; lesser movements were recorded at the upper half of the box since it was static in relation to the camera. Since the lower half of the shear box displaced 15 mm to the left, the bottom half of

375 the plot (see Fig. 6) displayed larger movements to the left. Localized activities were observed
376 as the displacement vectors evolved, where particles on the right end of the shear box moved
377 downwards and on the left end of the shear box, particles moved upwards. Such
378 micromechanical observations were found along the shear band by several authors during
379 discrete element modeling of granular materials (O'Sullivan et al. 2006; Kang et al. 2012;
380 Indraratna et al. 2014; Salazar et al. 2015) and during analysis of laboratory tests using PIV
381 technology (Peerun et al. 2015, Peerun et al. 2017). Activities such as dilation at the upper half
382 of the shear box and localized dilation at the bottom half of the shear box were also observed
383 in the vector plot (see Fig. 6). These observations are consistent to the work of Indraratna et al.
384 (2014) where it was demonstrated that shear bands actually developed as slanting planes as
385 opposed to the popular belief of being horizontal along the shear gap between the the top and
386 bottom halves of the shear box.

387 By showing the direct shear test and GeoPIV results side-by-side, an interpretation of the
388 particle behavior can be associated with the specimen strength characteristics at different
389 shearing stages. Localized particle activities such as compression and dilation were observed
390 and associated to their respective shear stress and volumetric plots. It is understood that
391 localized dilation would be due to particle interlocking while localized compression could be
392 due to possible particle breakages.

393 Fig. 7 (a) and (b) show the combination of direct shear testing and GeoPIV results for sand at
394 300 kPa normal stress, so as to gain better insight into the particle movements during the
395 shearing process. At the first stage of shearing, the volumetric plot showed almost no changes
396 in vertical displacement. This was portrayed in the Stage 1 vector plot where no vertical
397 movements were captured. Stage 2 showed an increase in shear stress until it reached peak state
398 and the specimen expanded to about 0.15 mm (dilation) and produced a dilatancy angle of 8.2^{o}.
399 The vector plot confirmed sample dilation where the vectors were moving to the left and in an

400 upward direction. Very similar upward and downward movements at the vicinities of the shear
401 box end walls were also identified as in the study of Indraratna et al. (2014). As described
402 earlier, Stage 2, known as particle interlocking will produce an increase in shear stress to
403 achieve peak state (Li and Aydin 2010). The vector plot portrayed localized compression
404 activities at the right end of the shear box along with an overall dilation through the shear box.
405 Such localized activities at the end of the shear band has been described previously by Shimizu
406 (1997) as localized strains in the end zones before peak stress is achieved. Indraratna et al
407 (2014) also described such compression as non-uniform volumetric strain which caused the
408 back of the shear box to compress while the front of the shear box to dilate. This could be due
409 to a contact force chain within the shear band where greater displacement and rotation occurs
410 to particles than those beyond the shear band. The third vector plot showed a reduction in
411 dilation, and hence, a reduction in shear stresses, as seen in Stage 3 of the shear stress plot.
412 Further dilation can be seen from the volumetric and vector plots. The last stage of shearing,
413 Stage 4, shows localized compression at the right end of the shear box, which is portrayed in
414 the volumetric plot. The upper half of the shear box showed minimal vertical movements,
415 whereas the bottom half was sheared to the left. The localized compression as shown on the
416 right end of the vector plot confirms the compression during the last stage of the volumetric
417 plot which also produced a reduction in shear stress instead of a steady shear.

418 ***Discussion***

419 *Effect of particle shapes on dilation and compression*

420 The sand specimen consisted of strong rounded and sub angular quartz particles that produced
421 more particle interlocking. Intense particle interlocking made the sample dilate and produced
422 higher peak stress as opposed to metagreywacke and shale. From Table 2, the dilatancy angle
423 of sand was relatively higher than the metagreywacke and shale samples. The metagreywacke
424 sample, consisting of angular particles, had relatively higher void ratio and the weak matrix of

425 fine-grained quartz, sericite, chlorite and clay minerals, was perhaps more susceptible to
426 particle deformations. Particle size distribution before and after shearing had been conducted
427 by Kim and Ha (2014), where they studied the effect of particle size on the shear behavior of
428 sand and gravel. The Particle Size Distribution (PSD) results before and after shearing showed
429 insignificant change; thus PSD could not conclusively indicate the degree of particle crushing.
430 Hence, in this study, the vector plots obtained from GeoPIV were used to identify localized
431 particle activities such as dilation and compression, which would possibly represent particle
432 interactions.

433 Figs. 8 (a) and (b) show the vector plots for sand and shale respectively, at Stage 3 under applied
434 normal stress of 300 kPa, where dilation was observed throughout the sand specimen as
435 opposed to shale. The sand specimen dilated due to particle interlocking, as seen in the upper
436 half of the shear box. Localized compression was recorded within shale specimen, which could
437 be due to particle deformations. This phenomenon would thus result in a reduction of shear
438 stresses (Indraratna et al. 2014) and reduction in dilation as observed in Fig. 8 (b). It was also
439 postulated from Fig. 8 (b) that any flaky mica minerals that had not undergone particle breakage
440 had realigned parallel to the shear zone, thus demonstrating significantly more frictional
441 behavior, thereby supporting the development of constant internal friction angles for shale.
442 Consistently, from the direct shear tests results, Fig. 4 (a) shows that sand at 300 kPa normal
443 stress, dilated to about 0.2 mm whereas Fig. 4 (c) shows shale was compressed to 0.55 mm
444 instead.

445 *Effect of particle shape on cohesion*

446 A specimen with higher void ratio and angular particles is more susceptible to deformations,
447 which will result in a reduction of the sample internal friction angle (Xiao et al. 2014). When
448 compared with metagreywacke and shale, sand exhibited larger apparent cohesion due to it
449 being well-graded and rounded with smooth surfaced particles, thus producing relatively lower

450 void ratio than the metagreywacke and shale. Higher shear stresses are produced due to greater
451 dilation caused by particle interlocking activities in sand and hence, contributes positively to
452 cohesion (Taylor, 1948). Based on this understanding, Fig. 9 (a) and (b) for sand as well as
453 metagreywacke and shale, respectively, at particle interlocking stage (σ'_n = 300kPa), are now
454 assessed. It was evident that micromechanical activities could be observed where particles
455 moved downwards towards the right end of the shear box while upwards particle movements
456 were captured towards the left end of the shear box. Such phenomenon was also evidently
457 observed by Indraratna et al. (2014), indicating that the development of the shear band is in
458 fact orientated at a slanting plane, rather than at a horizontal plane within the shear gap that
459 exists between the two halves of the shear box. This observation verifies the test results
460 obtained in this research, which uses both the purpose-built transparent shear box combined
461 with GeoPIV as a novel methodology to develop further understanding on particle behavior
462 during shearing.

463 The degree of interlocking activities for each material defines the apparent cohesion obtained
464 from the Mohr-Coulomb envelope. Sand exhibited the highest interlocking activities. It is
465 postulated that shale and metagreywacke were subjected to greater particle deformations during
466 Stage 1 due to the relatively greater compression, which subsequently reduced the interlocking
467 activities significantly. Reduction in interlocking activities as opposed to sand, produced
468 limited cohesion for metagreywacke and shale. Table 2 confirms that sand produced the highest
469 apparent cohesion, followed by metagreywacke spoils and zero apparent cohesion for the shale
470 spoils. Additionally, at σ'_n = 500 kPa, sand exhibited relatively larger dilatancy angle while
471 metagreywacke and shale exhibited contracting behavior.

472 *Effect of normal stress on cohesion*

473 Fig. 10 shows the peak power law strength envelope for well-graded sand, with tangential MC
474 failure criteria obtained using the generalized tangent technique at applied normal stresses of

475 100 kPa, 300 kPa and 500 kPa. At higher normal stress, soil specimens compressed and
476 interlocking amongst particles increased the shear strength of the sample (Xiao et al. 2014).
477 Similar observations were made for the sand and metagreywacke specimens, where increasing
478 normal stresses resulted in increasing tangential peak cohesion, $c'_{t,p}$ and reducing peak
479 tangential friction angle, $\phi'_{t,p}$. This confirms that at higher normal stresses, particle interlocking
480 (from apparent cohesion) was more significant than particle rolling (from friction) in
481 contributing to the shear strength of the tested specimens. Note that this observation applied to
482 non-linear strength behavior materials using the power law and tangential method. For the
483 linear behavior of shale, the MC envelope produced zero cohesion as shown in Fig. 5 (c). This
484 also suggests that particle shape and strength were factors in the degree of interlocking. As
485 mentioned above, the strong rounded quartz particles of sand had a lower void ratio and
486 produced the highest amount of dilation due to greater particle interlocking as opposed to
487 metagreywacke and shale. The relatively weaker and angular particles of metagreywacke and
488 shale had higher void ratio and made the specimens to compress due to possible particle
489 deformations. Hence, reduced interlocking produced lower and zero apparent cohesion for
490 metagreywacke and shale respectively.

491 The dilatancy angles for each specimen at the onset of peak shear stresses in reported in Table
492 2. Generally, the specimens compressed more with increasing normal stresses, as shown by the
493 reducing dilatancy angles. From the GeoPIV vector plots, similar observations were made for
494 the tested specimens. However, for greater clarity, only the vector plots for well-graded sand
495 are shown (see Fig. 11) and discussed, hereinafter.

496 These vector plots were obtained at the onset of peak shear stresses at each of the normal
497 stresses, which was the point where dilatancy angle was interpreted. At 100 kPa (see Fig. 11
498 (a)), the specimen demonstrated significant dilation as shown by the sub-vertical vectors
499 particularly in the top half of the ROI. Some dilatancy was also observed in the bottom half of

500 the ROI. At 300 kPa (see Fig. 11 (b)), slight localized compression was observed at the right
501 side of the top half of the ROI. Dilation was still observed throughout the specimen but
502 particularly in the top half of the ROI. There was minimal dilation in the bottom half of the
503 ROI. At 500 kPa (see Fig. 11 (c)), the specimen seemed to experience mainly reduced dilation
504 as compared to Figs. 11 (a) and (b). Almost no dilation was observed in the bottom half of the
505 ROI.

506 From the GeoPIV vector plots it can be seen that the particles needed to dilate in order to
507 overcome particle interlocking. The increasing normal stresses resulted in increased particle
508 interlocking, thus resulting in increased apparent cohesion. From the GeoPIV vector plots, this
509 increase in apparent cohesion was coupled with reducing dilation angles, owing to reduced
510 vertical movement and rolling of the particles. Therefore, this resulted in the reduction of
511 friction angles with increasing normal stresses.

512 ***Conclusions***

513 Particle behavior of sand, metagreywacke, and shale were studied in direct shear tests by means
514 of particle image velocimetry technique. Sand was classified as smooth, rounded to sub-angular
515 particles, while metagreywacke and shale were both classified as rough, angular particles.
516 Metagreywacke and shale consisted of relatively weaker matrices of fine-grain materials
517 cemented together, whereas the well-graded sand consisted mainly of relatively stronger quartz
518 particles. This study focused on providing better insights into particle behavior, which could
519 be used to explain the development of shear strength in different materials. Particle shape and
520 mineralogy were found to be of great influence on the development of apparent cohesion,
521 where strong rounded particles were seen to produce relatively greater apparent cohesion.

522 In this research, shear stress and volumetric plots were discussed in relation to the results
523 obtained from the PIV outputs. The following observations have been made:

a) Materials having rounded to sub-angular particles with relatively high quartz content produce relatively greater dilation behavior as opposed to fine-grained materials bound by relatively weaker matrices; b) Materials with angular particles and relatively high void ratio are more prone to compression; c) Greater dilation due to particle interlocking will produce greater apparent cohesion; d) Compression due to possible particle deformations will result in a reduction in peak shear stresses; e) At higher normal stresses, dilation due to particle interlocking produce greater apparent cohesion, while the magnitude of internal friction angle decreases with increasing normal stresses.

Using a purpose-built transparent shear box combined with reliable GeoPIV analyses as a novel methodology, this paper has successfully developed further understanding on particle behavior during shearing.

Acknowledgment

The authors would like to express their sincere thanks to Hock Seng Lee Bhd and Jurutera Jasa (Sarawak) Sdn Bhd for their generosity in providing access to field data, and to David White for the permission to use the GeoPIV software.

References

Adrian, R. J. (1991). "Particle imaging techniques for experimental fluid mechanics." *J. Fluid. Mech.*, 23261-304.

ASTM. (2011). "Standard practice for classification of soils for engineering purposes (unified soil classification system)", *D2487-11*, West Conshohocken, PA.

ASTM. (2011a). "Standard Test Method for Direct Shear Test of Soils Under Consolidated Drained Conditions." *D3080 / 3080M-11*, West Conshohocken, PA.

Bolton, M. D. (1986). "The strength and dilatancy of sands." *Geotechnique*, 36(1), 65-78.

547 Choo, C. S. (2015). "Develoment and Assessment of Equivalent Rock Strength Parameters for
548 the Back-analysis of Pipe-jacking Forces." *PhD thesis*, Swinburne University of
549 Technology Sarawak Campus.
550 Choo, C. S., and Ong, D. E. L. (2015). "Evaluation of Pipe-Jacking Forces Based on Direct
551 Shear Testing of Reconstituted Tunneling Rock Spoils." *J Geotech. & Geoenviron. Eng.*
552 doi:10.1061/(ASCE)GT.1943-5606.0001348
553 Choo, C. S., and Ong, D. E. L. (2017). "Back-analysis and numerical modelling of pipe-jacking
554 forces in the highly fractured and highly weathered Tuang Formation." Geotechnical
555 Research, *Institution of Civil Engineers*, UK. doi:http://dx.doi.org/10.1680/jgere.16.00022
556 Das, B. M. (2008). "Advanced soil mechanics." Third Edition edn, *Taylor & Francis*, London
557 and New York.
558 De Mello, V. F. B. (1977). "Reflections on design decisions of practical significance to
559 embankment dams." *Géotechnique*, 27(3), 281-354. doi:10.1680/geot.1977.27.3.281
560 DeGregorio, V. B. (1990). "Loading systems, sample preparation, and liquefaction." *J.*
561 *Geotech. Eng.*, 116(5), 805-821. doi:10.1061/(ASCE)0733-9410(1990)116:5(805)
562 DeJong, J. T., and Westgate, Z. J. (2009). "Role of initial state, material properties, and
563 confinement condition on local and global soil-structure interface behavior." *Journal of*
564 *Geotechnical and Geoenvironmental Engineering*, 135(11), 1646-1660.
565 doi:10.1061/(ASCE)1090-0241(2009)135:11(1646)
566 Djipov, D. N. (2012). "Effectes of particle breakage on the compression and shear behavior of
567 carbonate sand." *1st Civil and Env. Eng. Student Conference*, Imperial College London.
568 Fukuoka, H., Sassa, K., Wang, G., and Sasaki, R. (2006). "Observation of shear zone
569 development in ring-shear apparatus with a transparent shear box." *Landslides*, Springer-
570 Verlag, 3(3), 239-251. doi:10.1007/s10346-006-0043-2
571 Grognet, M. (2011). "The boundary conditions in direct simple shear tests, development for
572 peat testing at low vertical stress," *MSc thesis*, Delft University of Technology.

573 Indraratna, B., Ngo, N. T., Rujikiatkamjorn, C., and Vinod, J. S. (2014). "Behavior of fresh
574 and fouled railway ballast subjected to direct shear testing: discrete element simulation."
575 *Int. J. Geomech.*, 14(1), 34-44. doi:10.1061/(ASCE)GM.1943-5622.0000264
576 Kang, D. H., Lee, J. H., Choo, J., and Yun, T. S. (2012). "Pore directivity of soils subjected to
577 shearing: numerical simulation and image processing." *GeoCongress 2012*, pp. 2342-
578 2351. doi:10.1061/9780784412121.240
579 Kim, D., and Ha, S. (2014). "Effects of particle size on the shear behavior of coarse grained
580 soils reinforced with geogrid." *Materials*, 7963-979. doi:10.3390/ma7020963
581 Li, Y. R., and Aydin, A. (2010). "Behavior of rounded granular materials in direct shear:
582 Mechanisms and quantification of fluctuations." *Eng. Geology*, (115), 96-104.
583 doi:10.1016/j.enggeo.2010.06.008
584 Lu, N., Kim, T, Sture, S., and Likos, W. J. (2009). "Tensile strength of unsaturated sand." *Eng.*
585 *Mech*, (135), 1410-1419. 10.1061/(ASCE)EM.1943-7889.0000054
586 Mehdizadeh, A., Disfani, M. M., Evans, R., Arulrajah, A., and Ong, D. E. L. (2015).
587 "Discussion of “Development of an Internal Camera-Based Volume Determination
588 System for Triaxial Testing” by S. E. Salazar, A. Barnes and R. A. Coffman. The Technical
589 Note Was Published in Geotechnical Testing Journal, Vol. 38, No. 4, 2015. [DOI:
590 10.1520/GTJ20140249]," *Geotechnical Testing Journal*, (39), 165-168,
591 doi:10.1520/GTJ20150153
592 Mirzababaei, M., Mohamed, M., and Miraftab, M. (2017). "Analysis of strip footings on fiber-
593 reinforced slopes with the aid of particle image velocimetry." J. Mater. Civ. Eng, 29(4),
594 doi: 10.1061/(ASCE)MT.1943-5533
595 Oda, M., and Kunishi, J. (1974). "Microscopic deformation mechanism of granular material in
596 simple shear." *Japan Society of Soil Mech Foundation*, 14(4), 25-38.

597 Ong, D. E. L. and Choo, C. S. (2018). "Assessment of non-linear rock strength parameters for
598 the estimation of pipe-jacking forces. Part 1. Direct shear testing and backanalysis", *Eng.*
599 *Geol.*, 244 pp. 159-172, 10.1016/j.enggeo.2018.07.013.
600 Ong, D. E. L., and Choo, C. S. (2016). "Back-analysis and finite element modeling of jacking
601 forces in weathered rocks." *Tunnelling Underground Space Technol.*, (51), 1-10.
602 doi:10.1016/j.tust.2015.10.014
603 O'Sullivan, C., Bray, J. D., and Cui, L. (2006). "Experimental validation of particle-based
604 discrete element methods." *GeoCongress* pp. 1-18. doi:10.1061/40803(187)5
605 Peerun, I., Ong, D. E. L., and Choo, C. S. (2015). "Behaviour of reconstituted sand-sized
606 particles in direct shear tests using PIV technology." *Japanese Geotechnical Society*
607 *Special Publication*, 2 (8), 354-359, doi: 10.3208/jgssp.MYS-06
608 Peerun, M. I. (2016). "Behaviour of Reconstituted Sand-sized Tunnelling Rock Spoils during
609 Shearing using GeoPIV Technology for the Assessment of Soil Arching Effect during
610 Pipe-jacking Works." *MEng thesis*, Swinburne University of Technology.
611 Peerun, M. I., Ong, D. E. L. and Choo, C.S. (2016). "Calibration and Parametric Studies using
612 GeoPIV Technology to Track Particle Movements in a Transparent Shear Box", in DEL
613 Ong & CS Choo (eds.), Contributions of Young Geotechnical Engineers to Nation
614 Building – *Proceedings of the Young Geotechnical Engineers Conference 2016*, 30 May
615 2016, Selangor, Malaysia, ISBN 978-983-40616-5-4
616 Peerun, M. I., Ong, D. E. L., Choo, C. S., and Phangkawira, F. (2017). "Novel methods in
617 estimating pipe-jacking forces in highly fractured rocks." *NoDig India - Indian Society for*
618 *Trenchless Technology*, 13(1), 16-26.
619 Pfeffer, W. T. (2014), "Sedimentary rocks, CVN 3698 Engineering geology spring." *INSTAAR*
620 *Dept. Civil. Env. Architectural Eng*,University of Colorado.

621 Potts, D. M., Dounias, G. T., and Vaughan, P. R. (1987). "Finite element analysis of the direct
622 shear box test." *Géotechnique*, (37), 11-23.
623 Salazar, A., Sáez, E., and Pardo, G. (2015). "Modeling the direct shear test of a coarse sand
624 using the 3D Discrete Element Method with a rolling friction model." *Computers and*
625 *Geotechnics*, (67), 83-93. doi:10.1016/j.compgeo.2015.02.017
626 Sharma, J. S., Fleming, I. R., and Jogi, M. B. (2007). "Measurement of unsaturated soil-
627 geomembrane interface shear-strength parameters. " *Can. Geotech. J.* (44), 78-88.
628 doi:10.1139/T06-097
629 Shimizu, M. (1997). "Strain fields in direct shear box tests on a metal-rods model of granular
630 soils." In: Asaoka, Adachi, Oka. *Deformation and Progressive Failure in Geomechanics*,
631 151-156.
632 Taylor, D. W. (1948). "Fundamentals of soil mechanics), *John Wiley and Sons*, New York
633 Vangla, P. and Gali, M. L. (2016). "Effect of particle size of sand and surface asperities of
634 reinforcement on their interface shear behaviour. " *Geotextiles and Geomembranes*, (44)
635 254-268, doi.org/10.1016/j.geotexmem.2015.11.002
636 Wafiq, M. A., Sassa, K., Fukuoka, H. and Wang, G. H. (2004). "Evolution of shear-zone
637 structure in undrained ring-shear tests", *Landslide,* 1(2): 101-112, doi: 10.1007/s10346-
638 004-0001-9
639 Wang, G.H., and Sassa, K. (2002). "Post mobility of saturated sands in undrained load-
640 controlled rign shear tests", *Can Geotech J*, 3/9(4), 821-837, doi:10.1139/t02-032
641 White, D. J., and Take, W. A. (2002). "GeoPIV: Particle Image Velocimetry (PIV) software
642 for use in geotechnical testing", *Eng. Dept. Cambridge University*
643 White, D. J., Take, W. A. and Bolton, M. D. (2003). "Soil deformation measurement using
644 particle image velocimetry (PIV) and photogrammetry. " *Geotechnique*, (53), 619-631.

645 Xiao, Y., Liu, H., Chen, Y., and Jiang, J. (2014). "Strength and deformation of rockfill material
646 based on large-scale triaxial compression tests. I: Influences of density and pressure."
647 *Journal of Geotechnical and Geoenvironmental Engineering*, 140(12), 04014070.
648 doi:10.1061/(ASCE)GT.1943-5606.0001176
649 Yang, X. L., and Yin, J. H. (2004). "Slope stability analysis with nonlinear failure criterion."
650 *J. Eng. Mech.*, 130(3), 267-273. doi:10.1061/(ASCE)0733-9399(2004)130:3(267)
651 Yuan, Q., Wang, Y. H., Tam, P. O., Li, X., and Geo, Y. (2017). "Experimental
652 Characterizations of Contact Movement in Two-Dimentional Rod Assembly Subjected to
653 Direct Shearing", *Int. J. Geomech.*, 17(1), doi: 10.1061/(ASCE)GM.1943-5622.0000685

Table 1. Physical properties of samples tested

Specimen	D_{60} *(mm)*	D_{30} (mm)	D_{10} (mm)	D_{av} (mm)	Coefficient of uniformity C_u	Coefficient of curvature C_c	Dry density (kg/m^3)	Material classification (ASTM 2011)
Sand	0.70	0.27	0.10	0.60	7.00	1.04	1,995	Well-graded sand
Metagrey-wacke	0.65	0.28	0.15	0.48	4.33	0.80	1,878	Poorly graded sand-sized spoils
Shale	0.90	0.40	0.20	0.70	4.50	0.89	1,819	Poorly graded sand-sized spoils

Table 2. Comparison of results of peak and residual shear strength for sand, metagreywacke and shale

Material	Tangent at confining pressure (kPa)	Dilatancy angle, ψ (°)[a]	Apparent cohesion c' (kPa)		Internal friction angle ϕ' (°)	
			Peak	Residual	Peak	Residual
Well-graded Sand	100	8.2	14.7	4.1	39.4	30.9
	300	6.4	37.3	11.5	34.8	29.2
	500	4.1	57.5	18.6	32.8	28.4
Metagreywacke	100	3.8	9.5	0.8	37.7	35.0
	300	0.7	25.3	2.2	34.7	34.5
	500	-0.2	39.8	3.7	33.0	34.5
Shale[b]	100	2.4	0.0	0.0	37.3	35.0
	300	2.0	0.0	0.0	37.3	35.0
	500	-0.1	0.0	0.0	37.3	35.0

Note: [a]Measured at occurrence of peak shear stresses.

[b]Line of best fit was sufficient to develop M-C failure criterion.

Table 3. Void ratio before and after shearing of tested specimens

Specimen	Normal Stress (kPa)	Volume of Specimen (m^3)	Weight of Specimen (Kg)	Initial Void Ratio	Change in Void Ratio	Void Ratio after Shearing
Sand	100	0.0000852	0.170	0.353	0.005	0.358
	300				0.001	0.354
	500				-0.002	0.351
Metagreywacke	100		0.160	0.438	0.005	0.443
	300				-0.013	0.424
	500				-0.024	0.414
Shale	100		0.155	0.484	-0.004	0.480
	300				-0.016	0.468
	500				-0.029	0.455

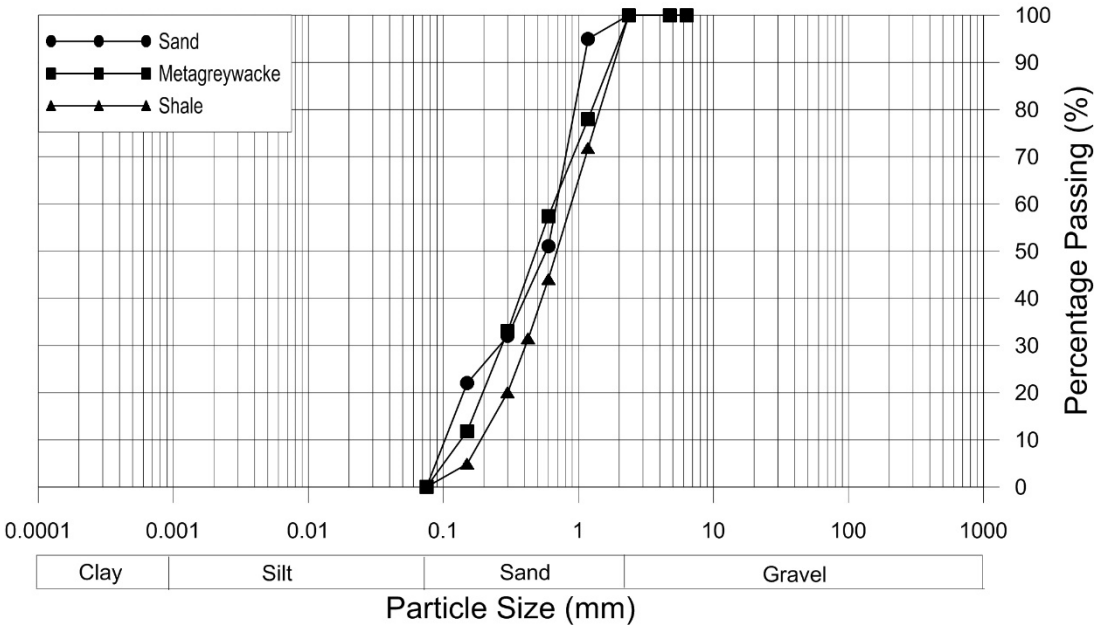

Fig. 1. Particle size distribution curve for sand, metagreywacke, and shale.

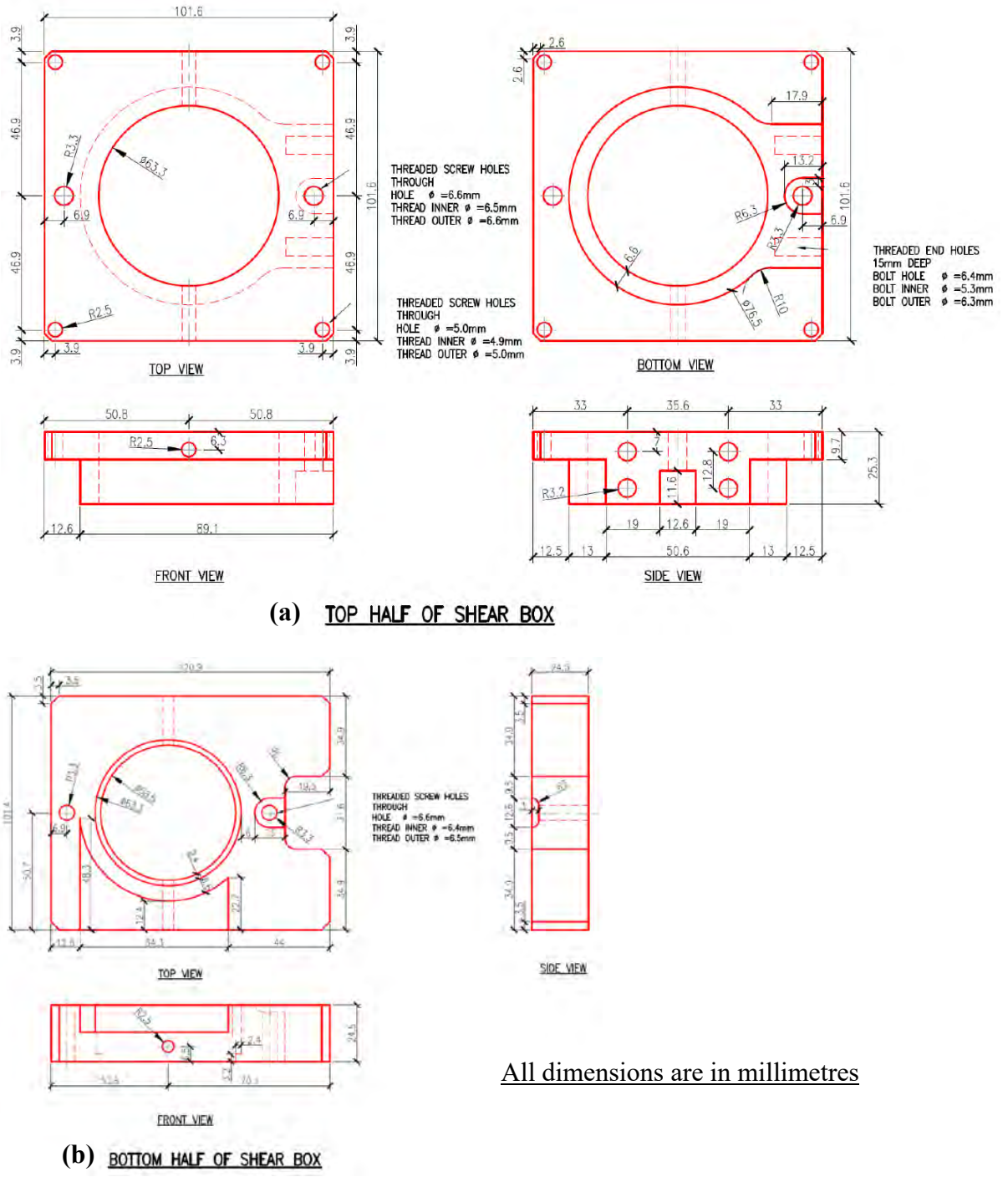

Fig. 2. Drawing specifications of (a) top half and (b) bottom half of the Perspex shear box

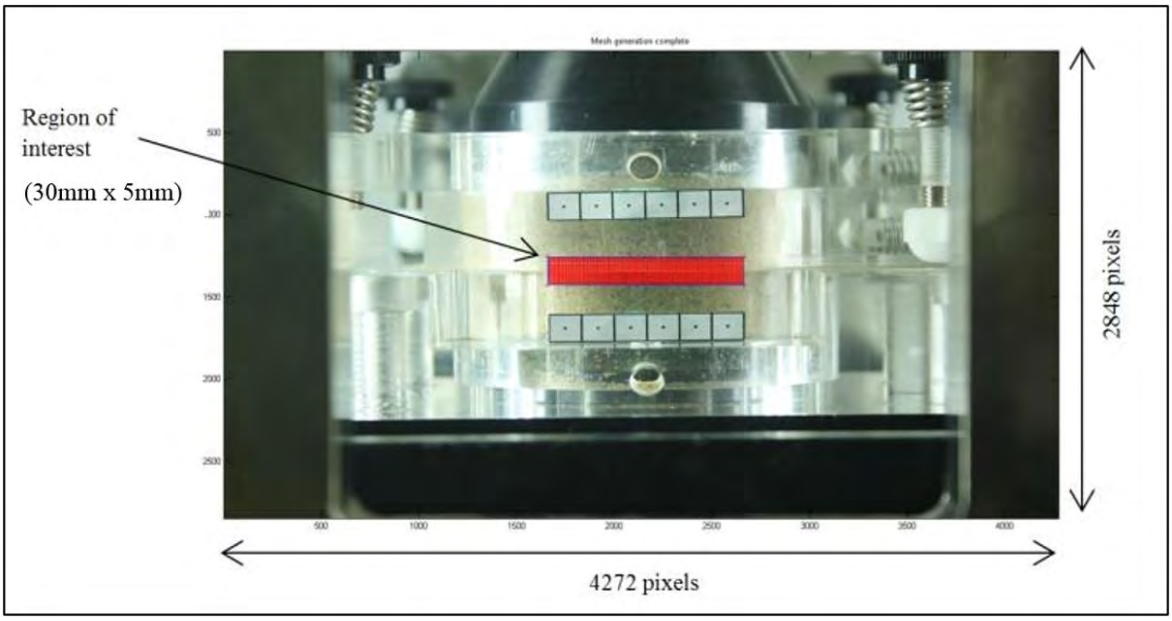

Fig. 3. Image acquisition with highlighted region of interest

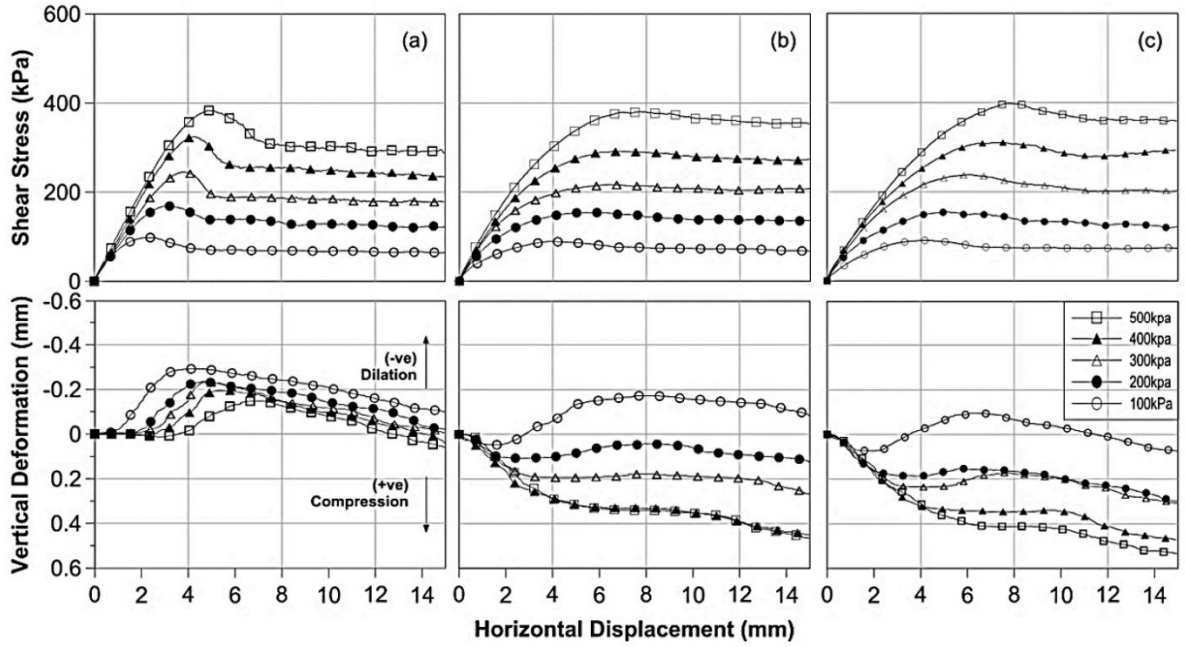

Fig. 4. Results of direct shear testing for (a) well-graded sand, (b) sand-sized spoils of metagreywacke and (c) sand-sized spoils of shale

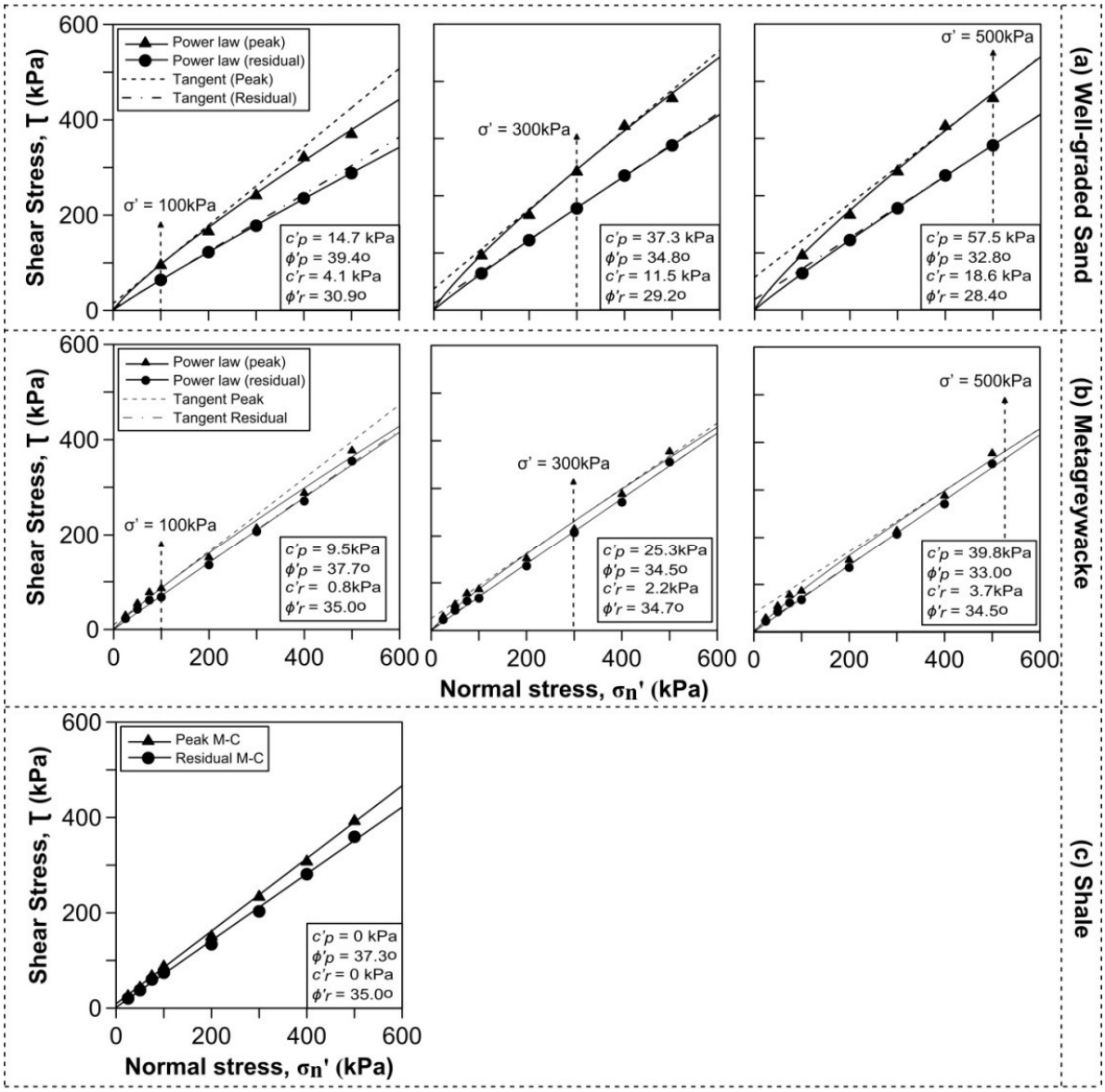

Fig. 5. Non-linear behavior of (a) sand, (b) metagreywacke at normal stresses of 100 kPa, 300 kPa and 500 kPa and (c) Mohr-Coulomb behavior for shale

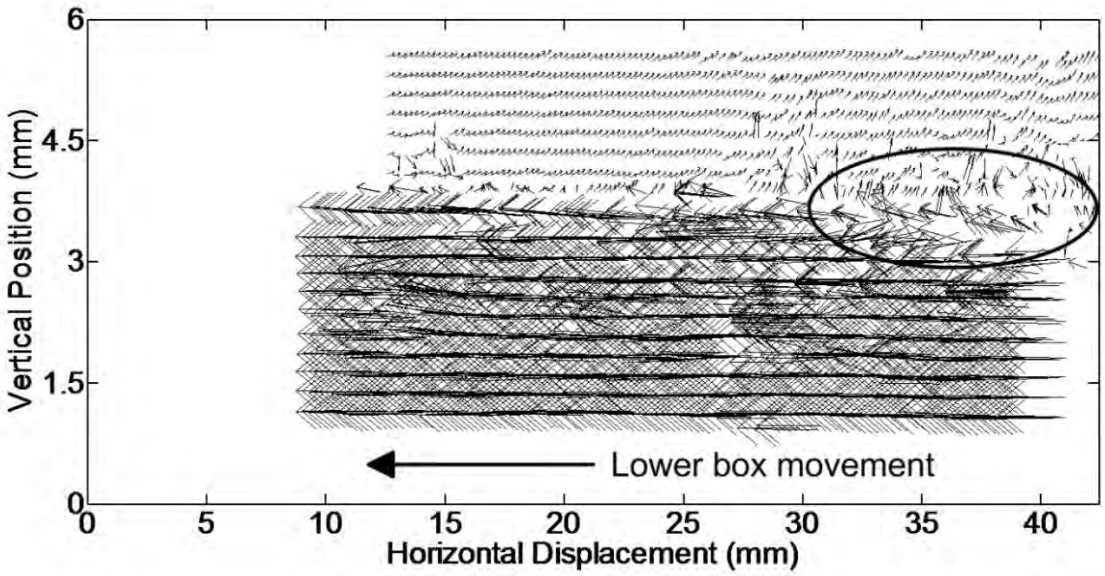

Fig. 6. Typical vector plot of well-graded sand (σ'_n = 500kPa) at Stage 3 showing localized dilation

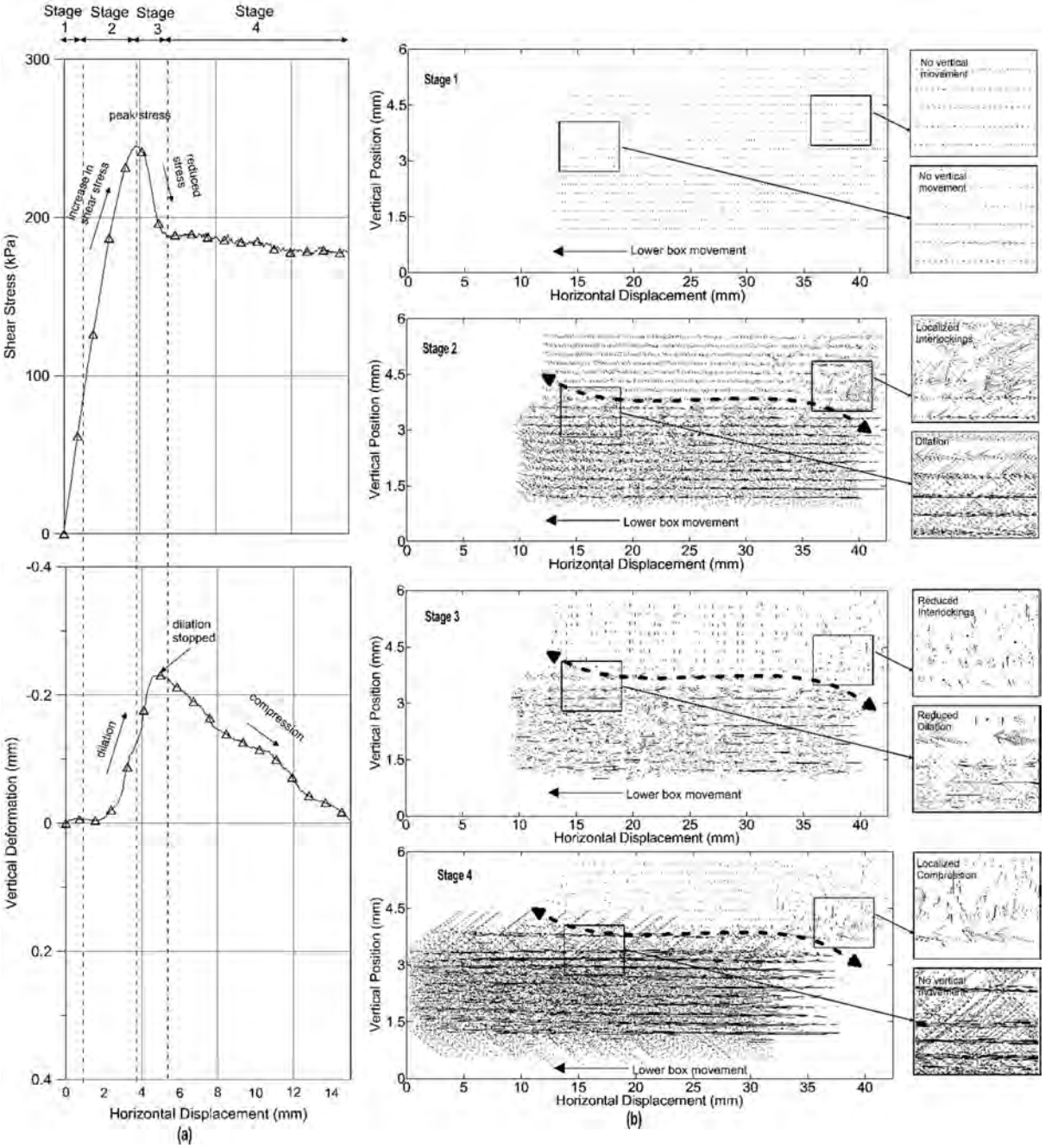

Fig. 7. (a) Direct shear test results and (b) vector plots for each shearing stage of sand at 300 kPa normal stress

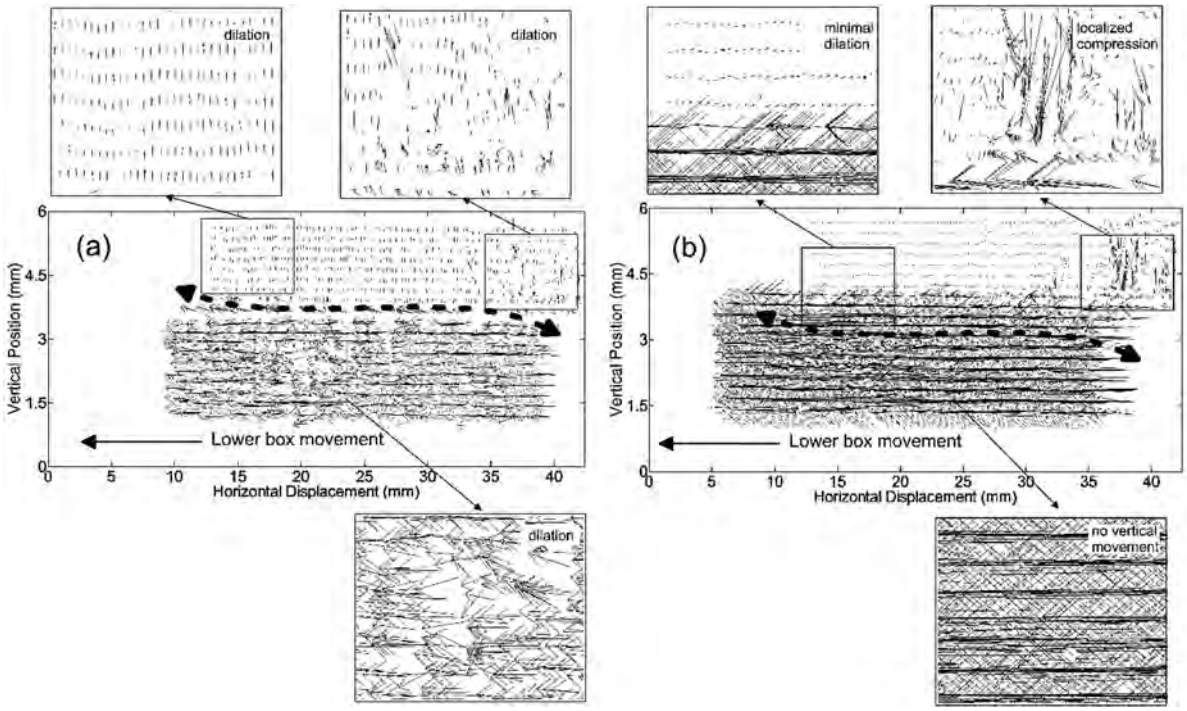

Fig. 8. Vector plots showing localized interlocking for (a) sand and (b) shale at Stage 3 and normal stress of 300 kPa

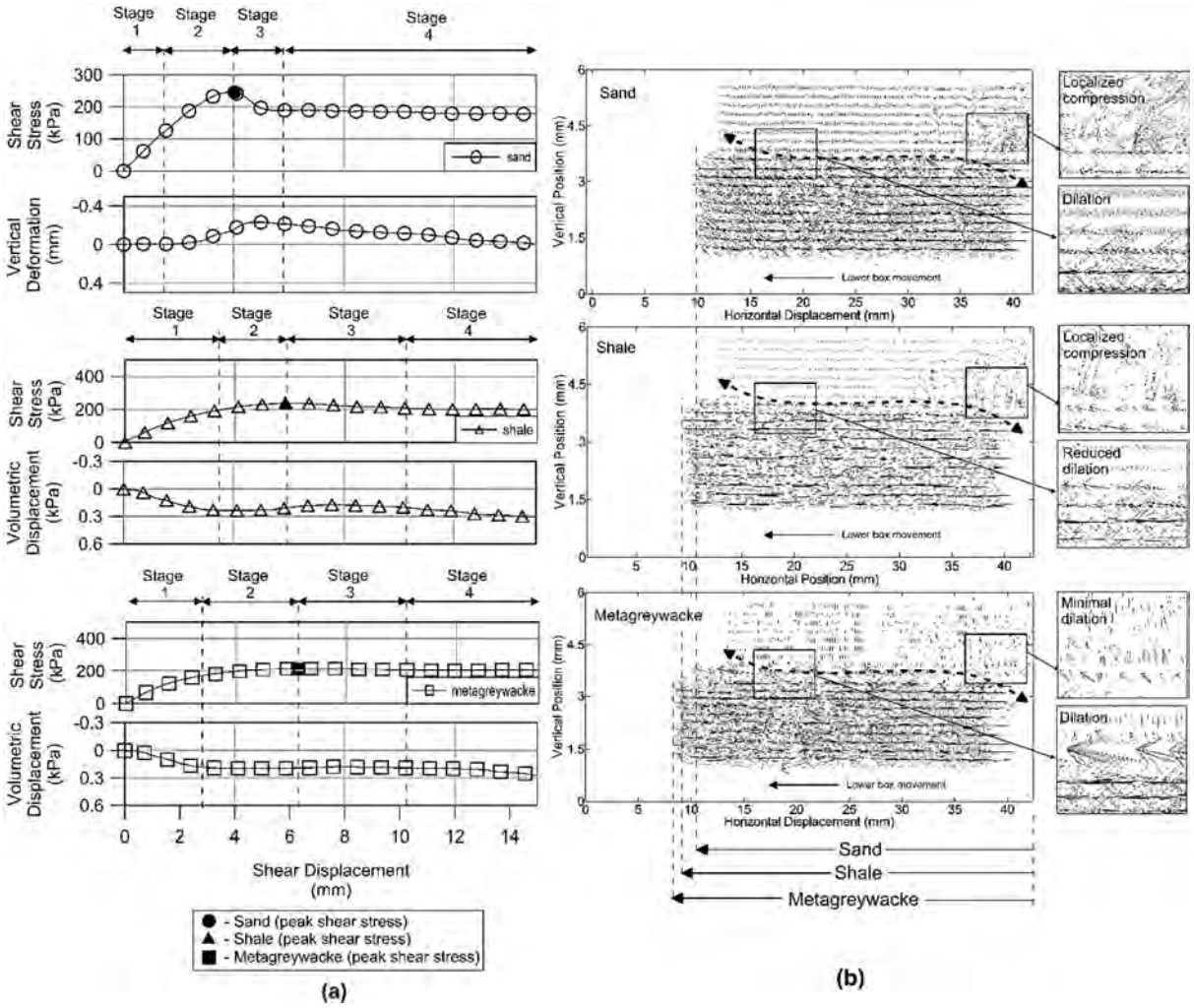

Fig. 9. (a) Mobilized peak shear stresses and (b) vector plots at Stage 2 shearing for sand, shale and metagreywacke at normal stress of 300 kPa

Figure 10

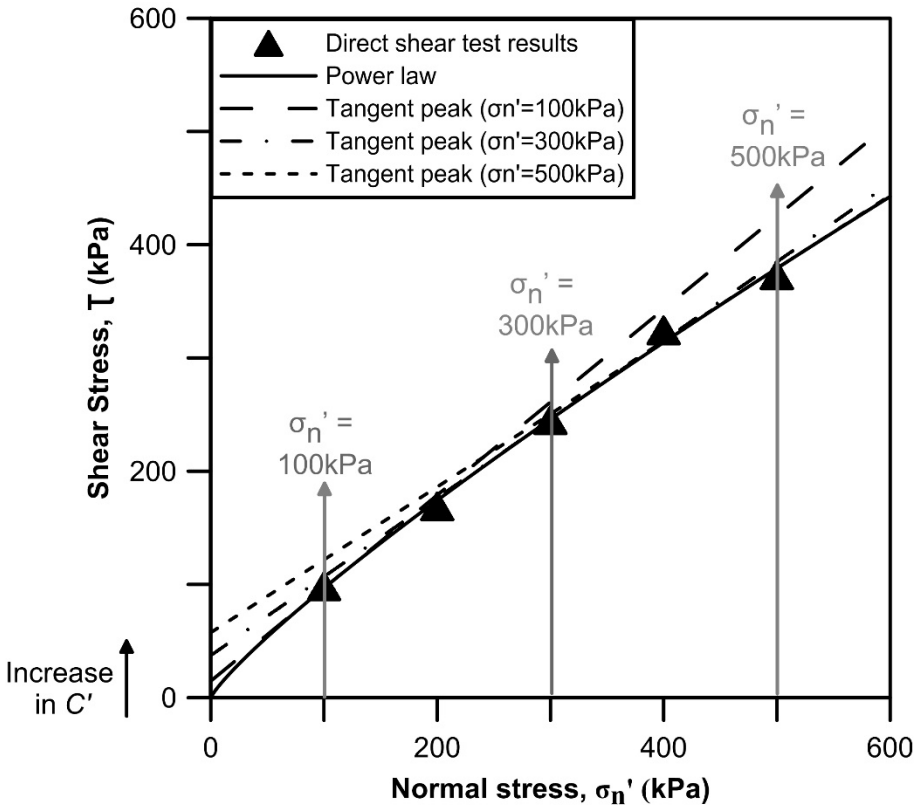

Fig. 10. Effect of increasing normal stresses on apparent cohesion, *c'* for well-graded sand

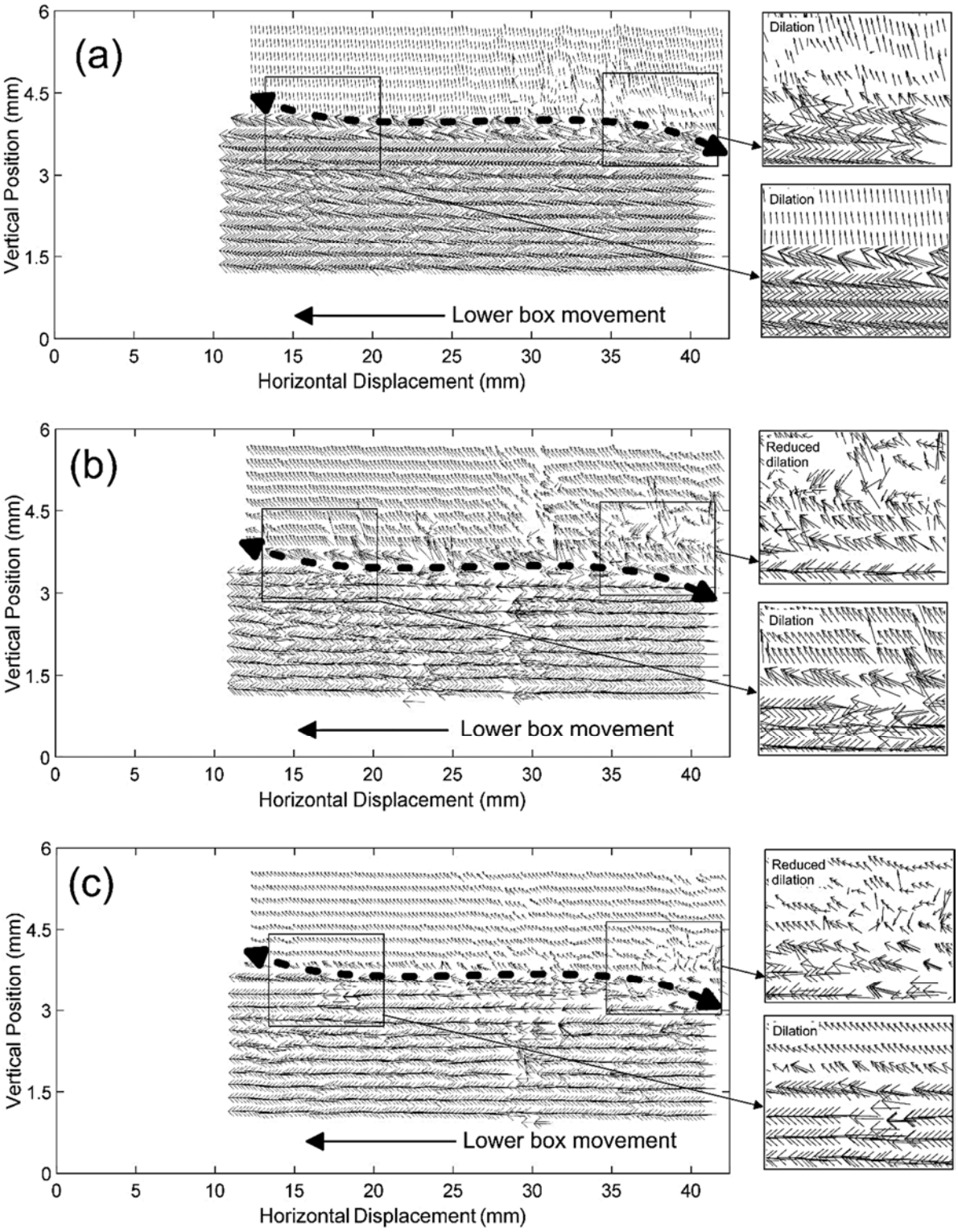

Fig. 11. Dilation due to interlocking activities for sand during peak shear stress at normal stresses of (a) 100 kPa, (b) 300 kPa and (c) 500 kPa

List of Figures